ACS APPLIED MATERIALS & INTERFACES

RESEARCH ARTICLE

www.acsami.org

Effect of Thermally Reduced Graphene Sheets on the Phase Behavior, Morphology, and Electrical Conductivity in Poly[(α-methyl styrene)-co-(acrylonitrile)/poly(methyl-methacrylate) Blends

Giovanni Vleminckx,[†] Suryasarathi Bose,[†,∥] Jan Leys,[‡] Jan Vermant,[†] Michael Wübbenhorst,[‡] Ahmed A. Abdala,[§] Chris Macosko,[⊥] and Paula Moldenaers*[,†]

[†]Department of Chemical Engineering and Leuven Materials Research Center, Katholieke Universiteit Leuven, Willem de Croylaan 46, B-3001, Leuven, Belgium

[‡]Department of Physics and Astronomy, Katholieke Universiteit Leuven, Celestijnenlaan 200D, B-3001, Leuven, Belgium

[§]Department of Chemical Engineering, The Petroleum Institute, POB 2533, Abu Dhabi, United Arab Emirates

[⊥]Department of Chemical Engineering and Materials Science, University of Minnesota, Minneapolis, Minnesota 55455-0331, United States

ABSTRACT: The effects of thermally reduced graphene sheets (TRG) on the phase separation in poly[(α-methyl styrene)-co-(acrylonitrile)]/poly(methyl-methacrylate) blends were monitored using melt rheology, conductivity spectroscopy, and electron microscopic techniques. The TRG were incorporated in the single-phase material by solution mixing. The composite samples were then allowed to phase separate in situ. The thermodynamics of phase separation have been investigated by monitoring the evolution of the storage modulus (G') as a function of temperature as the system passes through the binodal and the spinodal lines of the phase diagram. The phase separation kinetics were probed by monitoring the evolution of G' as a function of time at a quench depth well in the spinodal region. It was observed that TRG significantly influenced the phase separation temperature, the shape of the phase diagram and the rate of phase separation. The state of dispersion of TRG in the blends was assessed using electron microscopy and conductivity spectroscopy measurements. Interestingly, the composite samples (monophasic) were virtually insulators at room temperature, whereas highly conducting materials were obtained as a result of phase separation in the biphasic materials.

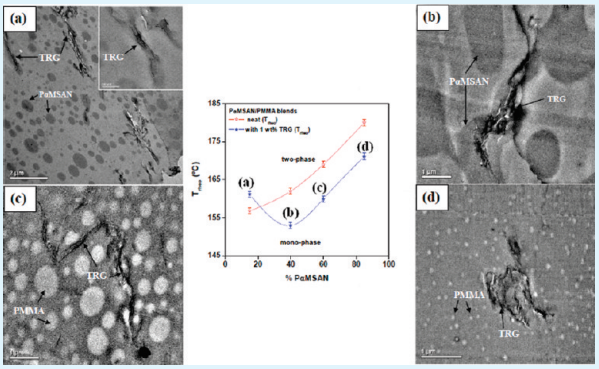

KEYWORDS: phase separation, thermally reduced graphene sheets, melt-rheology, morphology, electrical conductivity

INTRODUCTION

The advent of polymer blends has gained a lot of interest in the past decades. More recently, the addition of nanoparticles (NPs) to polymer blends has come under intense study as the NPs offer "synergistic" effects in the blends (for a recent review, see refs 1 and 2) they also offer a method to control the morphological features in the blends.[3,4] While a wide range of NPs in immiscible polymer blends has been explored, the effect of their presence in partially immiscible blends is not yet fully understood. Phase separation in polymer blends is of scientific as well as practical interest as different mechanisms of phase separation yield different morphologies[5] and can in turn be used as a scaffold for organizing the nanoparticles in the blend.

Over the years, various techniques have been explored to probe the phase separation in polymer blends. The most commonly used are optical[6] and scattering techniques.[7] However, probing the phase separation in polymer blends in the presence of NPs limits the use of these techniques as multiple scattering becomes dominant and the turbidity is too high. In this context, rheological measurements[8−13] can serve as an alternative tool in probing the phase separation in such complex materials. However, understanding the rheological behavior in the vicinity of phase separation still remains a challenge. Polymer blends that phase separate from the one-phase regime through the metastable regime to the two-phase regime, exhibit interesting rheological behavior. Significant changes are observed in the linear viscoelastic properties when a polymer blend is heated or cooled for lower critical solution temperature (LCST) and upper critical solution temperature (UCST) blends respectively. The temperature at which this transition occurs typically depends on the blend composition,[10] but shear flow can also interfere with both the thermodynamics and kinetics of phase separation. Hence, the critical temperature can also be affected together with the rheological material functions, due to applied stresses

Received: May 25, 2011
Accepted: July 12, 2011
Published: July 12, 2011

and strains, although their influence is limited as long as the strain amplitude is in the linear viscoelastic range.[14] In recent studies, it has been shown that the apparent binodal point shifts to higher temperatures when the frequency of the oscillatory measurements is increased. Moreover, oscillatory shear even at low frequency might accelerate the coagulation or growth of the domains although it might not affect the critical point of phase separation.[15,16]

The phase separation temperatures can be determined through isochronal dynamic temperature ramp measurements. For LCST blends, at low temperatures (in the homogeneous region), G' decreases with temperature as a result of increased mobility of polymer chains above the glass transition temperature. In the vicinity of the phase separation temperature, a competing effect from thermodynamic forces on the chain mobility arises and on further increasing the temperature, the increase in thermodynamic concentration fluctuations slows down. As thermodynamic forces become dominant, an upturn is observed in G' versus temperature.[17] The binodal (T_b) and the rheological phase separation temperature (T_{rheo}) can be quantitatively estimated through the onset and the inflection point of the upturn in G′ respectively.[14] In addition, the T_b can also be estimated using change in slope of the loss angle ($\tan \delta$) with respect to the temperature.[18] The spinodal temperature (T_s) on the other hand, can be determined by constructing Fredrickson-Larson plots which were developed to detect the order−disorder transitions in block copolymers through mean field theory.[19] Later, this was extended to polymer blends by Ajji and Choplin.[8] Rheological measurements have also been used as a probe to get insight in the morphological changes during phase separation, both under quiescent and shear flow conditions. The temporal evolution of the dynamic moduli (G' and G'') shows an increase or decrease depending on the changes in morphology. In case of cocontinuous structures the initial increase is commonly attributed to the formation of a highly interconnected network, whereas the subsequent decrease is associated with the loss of interconnectivity due to coarsening or break-up of initially formed cocontinuous structures.[14]

The high specific surface area associated with nanoparticles (like carbon nanotubes, clay, silica, etc.) enhances the chances of adsorption of macromolecular chains onto their surface. This phenomenon has been identified to be partially irreversible in nature.[20] As a direct consequence of the adsorption, the nanoparticles can influence the structural evolution, phase separation and final state of dispersion of the nanoparticles in the polymer blend. Ginzburg[21] proposed a simple comprehensive theory to explain the effects of spherical NPs on the phase separation. Later on, this theory was extended to rod-like particles.[22] Ginzburg predicts that for LCST-type blends, when NPs are preferentially adsorbed by macromolecular chains, an increase in the filler concentration leads to a shift in phase separation temperatures to higher temperatures, especially when the radius of the NPs is smaller than the radius of gyration of the polymers. This was explained by the reduction of unfavorable polymer−polymer interactions in favor of polymer−particle interactions. Furthermore, for NPs with radius larger than the radius of gyration of the polymer a downward shift in the spinodal decomposition temperature has been predicted by this model.[21] The adsorption of macromolecular chains onto the surface of the NPs can also slow down the phase separation kinetics by retarding the domain growth and arresting domain coarsening.[23] In addition, recent investigations revealed that nanorods are much more effective in slowing down the kinetics than nanospheres and can even inhibit the phase separation process leading to a long-lived kinetically trapped state.[24]

Graphene-based polymeric composites has come under intense study. Recently, it was shown that rapid thermal expansion of completely oxidized graphite oxide produces a high surface area material known as thermally reduced graphene sheets (TRG).[25] The single sheets were observed to have a wrinkled topology. It is envisaged that the nanoscale surface roughness (i.e., wrinkled topology) and the oxygen functionalities in TRG allow enhanced interactions with the polymeric matrix and consequently better thermal and mechanical properties.[26] A recent review addresses the current research on graphene/polymer nanocomposites.[27] However, the effects of TRG on the phase separation of polymer blends have not been investigated yet (at least not to our knowledge).

This paper systematically investigates the effects of TRG on the thermodynamics and kinetics of phase separation in an LCST blend by using melt-rheology as a probe. The concentration of TRG chosen here is well below the rigidity percolation threshold which was determined a priori by small amplitude oscillatory measurements. The evolution of the linear viscoelastic storage modulus (G') will be monitored as a function of temperature to investigate the thermodynamics of phase separation and to construct a phase diagram. Time evolution of G' at a quench depth well in the spinodal regime will be monitored to study the effect of TRG on the kinetics of phase separation. The state of dispersion of TRG in the blends will be assessed by electron microscopy and by monitoring the evolution of electrical conductivity during the phase separation process.

2. EXPERIMENTAL SECTION

2.1. Materials. Blends of poly[(α-methyl styrene)-co-acrylonitrile] (PαMSAN) and poly[methyl-methacrylate] (PMMA) (a typical LCST blend) have been used here. Both PαMSAN (Luran KR2556) and PMMA (Lucryl G77) were obtained from BASF. An overview of the characteristics of these polymers and the phase behavior of the blends has been extensively discussed by Laun.[6] The viscoelasticity of the components (PαMSAN, PMMA) at 210 °C is almost identical. For the 40/60 PαMSAN/PMMA and 60/40 PαMSAN/PMMA blends cocontinuous morphologies are expected, whereas the 15/85 PαMSAN/PMMA and 85/15 PαMSAN/PMMA blends are expected to show matrix-droplet morphologies. For this model system it has been reported that homogeneous mixtures that phase separate into a droplet-matrix morphology will display an increase in elasticity at low frequencies because of the development of a dispersed droplet phase (dominant interfacial aspects) whereas the blends that phase separate into a cocontinuous structure will show a decrease in elasticity in the late stages of phase separation (due to loss in interconnectivity of the domains).[28]

Thermally reduced graphene sheets (TRG, as synthesized) were kindly provided by Prof. Ahmed Abdala (The Petroleum Institute, UAE). TRG are prepared by reduction of graphite oxide. Nevertheless, the final reduced sheets still contain significant amounts of oxygen. The term reduced is used relative to graphite oxide and it refers to the change of the carbon/oxygen atomic ratio from 2/1 for graphite oxide to about 10/1 for reduced graphene. The details related to expansion and exfoliation of graphite together with the characterization of TRG have been discussed in detail by McAllister et al.[29] The functionalization together with the exfoliation results in stacked structures of graphene which causes the specific surface area to be higher than that of graphite (600−900 m^2/g).[29] The TRG have a mean thickness of the order

of 1.75 nm and a characteristic length scale in the range of 100 nm to 2.5 μm.

2.2. Sample Preparation. TRG based composites were prepared using solution mixing. The required amount of TRG was dispersed in 10 mL of tetrahydrofuran (THF) by bath sonication (Elmasonic S 100H, 37 kHz, 600 W power setting, effective power: 150W) at room temperature. These solutions were then combined with a solution of PαMSAN/PMMA in THF (10−30 mL) to yield a total composite mass of 2 g. Shear mixing (IKA Ultra-Turrax T25) at 8,000 rpm was subsequently applied to the PαMSAN/PMMA/TRG composites for 45 min. The composite solution was precipitated in methanol (400 mL) and filtered under vacuum using a Teflon coated glass filter (Winzer, Germany with pore size 4, diameter: 10−16 μm), and dried at 80 °C for 12 h to yield a solid flaky material. The unfilled PαMSAN/PMMA blends were also prepared in the same way to eliminate possible artifacts.

2.3. Characterizations. The viscoelastic properties of the blends were measured using an AR2000ex stress-controlled rheometer (TA Instruments, New Castle, DE) with parallel plate geometry (25 mm diameter and 1 mm gap) under N_2 atmosphere. Isochronal dynamic temperature ramp measurements were performed at a uniform heating rate of 1.0 °C/min from the single phase (120 °C) to the phase separated regime (220 °C) to detect the onset of phase separation in the blends. A fixed frequency (0.1 rad/s), which is low enough to lie in the terminal regime (determined a priori for neat blends and composite samples),[6] was applied and the strain amplitude was verified to be within the linear viscoelastic region.

To investigate the kinetics of phase separation, we performed time-sweep experiments after a temperature jump from room temperature to 220 °C. Strain was 1% and frequency 0.1 rad/s. After 5 h, the blends morphology was characterized in more detail by small amplitude oscillatory measurements as a function of frequency.

Transmission electron microscopy (TEM) was performed on a FEI Tecnai T12 microscope using an accelerating voltage of 100 kV. Samples of 15/85, 40/60, 60/40 and 85/15 PαMSAN/PMMA blends with 1 wt % TRG were allowed to phase separate for 5 h at high temperature (220 °C) and subsequently quenched in a cold water bath to freeze the morphology. Thin sections of 100 nm were cut with a microtome at room temperature and then picked up in carbon-film coated Cu grids. To increase the contrast for the images of the 85/15 PαMSAN/PMMA blend, the sample was stained by RuO_4 aqueous solution (0.5%) for 5 min.

Conductivity spectroscopy measurements were performed both at room temperature and at an elevated temperature of 220 °C on the compression molded samples (16.5 mm diameter and 1.75 mm thickness) in the frequency range of 1×10^{-1} to 1×10^{7} Hz using a Novocontrol Alpha high-resolution dielectric analyzer. The instrument measures the complex impedance of the sample; knowing the geometry of the sample the complex conductivity can be calculated. In this work, the real part of the complex conductivity will be used. For the conductivity spectroscopy measurements at 220 °C, the samples were placed between two brass plates, separated by an annular Teflon spacer to maintain the sample geometry in the melt state. The same spacer was used for all the measurements in order to avoid errors due to differences in sample dimensions. The temperature was controlled by a Novocontrol Quatro temperature controller, which uses a nitrogen gas flow to control the sample temperature with an accuracy of 0.1 °C. Frequency scans were performed at 220 °C during 5 h, i.e., each frequency scan took about 3 min to complete, and 100 such scans were performed. Further details about the dielectric instrumentation and data analysis can be found in ref 30−32.

3. RESULTS AND DISCUSSION

3.1. Thermodynamics of Phase Separation: Effect of TRG on the Phase Diagram. In general, the phase separation temperature or the cloud point temperature in polymeric blends are often determined using optical (light microscopy) methods. However, neither the one-phasic blends with nanoparticles nor the phase separated samples are translucent, which makes it difficult to evaluate cloud point temperature using optical methods. In this context, melt-rheology can serve as a useful tool to probe the phase separation temperatures in such complex materials. As mentioned in the Experimental Section, TRG (1 wt %) were incorporated in the one phasic system by solution mixing. The samples were then allowed to phase separate at an elevated temperature in the rheometer in situ. Previous investigations[10,15,17,33] have reported that the phase separation

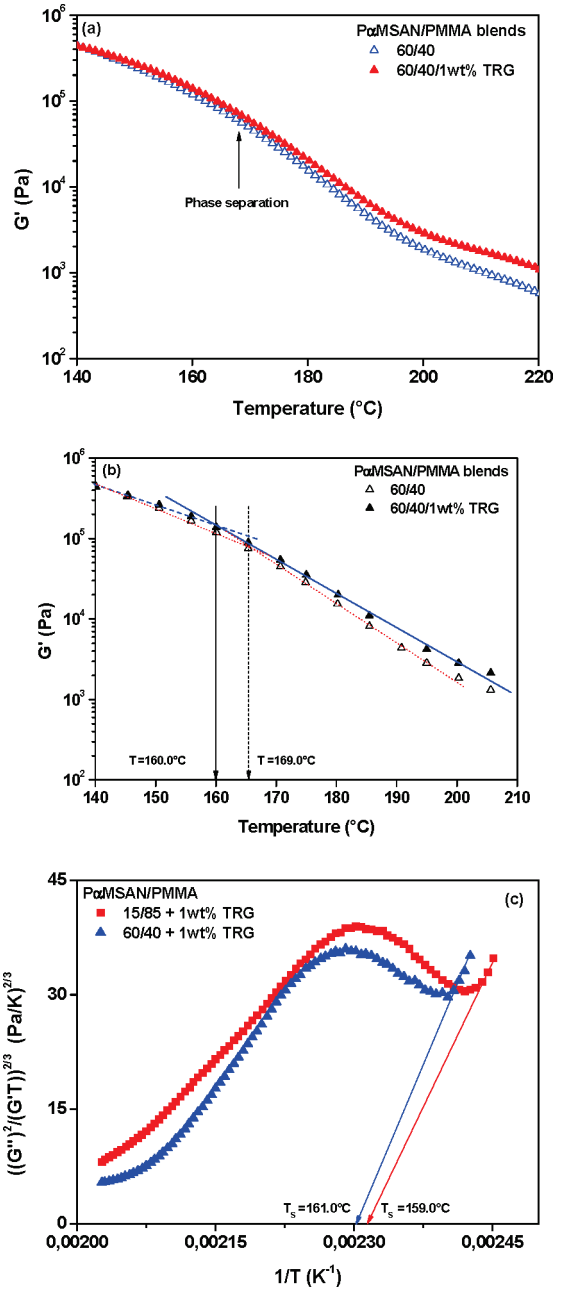

Figure 1. (a) Dynamic temperature ramps at 1 °C/min; (b) determination of T_{rheo} for the 60/40 PαMSAN/PMMA blends with and without TRG; (c) Fredrickson Larson plots for 15/85 and 60/40 PαMSAN/PMMA blends with TRG.

Table 1. Rheological Phase Separation Temperature T_{rheo}, Spinodal Phase Separation Temperature T_s, Optically Determined Phase Separation Temperature T_{opt}, and Phase Separation Temperature T_{ann} Determined through Annealing Experiments for the Different Samples

	Sample	T_{rheo} (±1 °C)	T_s(from eq. 4) (±2 °C)	T_{opt}[6]	T_{ann}[6]
15/85	neat	157	150	<160	≤150
	1 wt % TRG	161	159		
40/60	neat	162	151	165	160
	1 wt % TRG	153	147		
60/40	neat	169	158	175	170
	1 wt % TRG	160	161		
85/15	neat	180	194	190	
	1 wt % TRG	171	191		

temperature, often termed as the rheological phase separation temperature (T_{rheo}), can be determined by monitoring the evolution of the G′ as a function of temperature. As the temperature is elevated, the system moves away from the glass transition temperature (T_g) and G' decreases because of an increased chain mobility (Brownian motion). As the temperature is raised further and in the vicinity of the critical point (i.e., phase separation), a clear change in slope is often observed (see Figure 1a) depending on the dynamic asymmetry (contrast in the T_g) of the components and the interfacial tension. This slope change is a result of the competition between mobility and thermodynamics. At higher temperatures, deep in the spinodal regions, the thermal motion again dominates the viscoelastic properties of the blends again. Using the slope change in G' versus temperature, we determined T_{rheo} for all the samples (see Table 1). As an example, the determination of T_{rheo} for 60/40 PαMSAN/PMMA blends with and without TRG is shown in Figure 1b.

From the dynamic temperature ramp measurements, one can also determine the binodal (T_b) and the spinodal phase separation temperature (T_s) by using the theoretical approach of Fredrickson and Larson[19] which was later on extended by Ajji and Choplin[34] for polymer blends in the vicinity of phase separation. The theory yields the following expressions for the dynamic storage (G') and loss moduli (G'') in the terminal regime, respectively

$$G' = \frac{k_B T\omega^2}{1920\pi}\left[\frac{1}{3}\left\{\frac{R_{g1}^2}{\phi N_1} + \frac{R_{g2}^2}{(1-\phi)N_2}\right\}\right]^{1/2} \times \left[\frac{1}{\phi a_1^2 W_1} + \frac{1}{(1-\phi)a_2^2 W_2}\right]^2 [2(\chi_s - \chi)]^{-5/2} \quad (1)$$

$$G'' = \frac{k_B T\omega}{240\pi}\left[\frac{1}{3}\left\{\frac{R_{g1}^2}{\phi N_1} + \frac{R_{g2}^2}{(1-\phi)N_2}\right\}\right]^{-1/2} \times \left[\frac{1}{\phi a_1^2 W_1} + \frac{1}{(1-\phi)a_2^2 W_2}\right]^2 [2(\chi_s - \chi)]^{-1/2} \quad (2)$$

where ϕ is the volume fraction of polymer 1, χ is the interaction parameter and χ_s designates the interaction parameter at the spinodal point. R_{gi} denotes the radius of gyration of species i, N_i is the number of segments, W_i is the rate of motion of the subunit of length a_i. Assuming the following expression for the interaction parameter χ

$$\chi = A + \frac{B}{T} \quad (3)$$

the following expression can be obtained

$$\left(\frac{G''^2}{TG'}\right)^{2/3} = \frac{B}{C}\left(\frac{1}{T_s} - \frac{1}{T}\right) \quad (4)$$

where C is given by

$$C = \left(\frac{45\pi}{k_B}\right)^{2/3}\left[\frac{a_1^2}{\phi} + \frac{a_2^2}{(1-\phi)}\right] \quad (5)$$

A linear relationship can be obtained by plotting $(G''^2/TG')^{2/3}$ versus $(1/T)$ and the intercept with the horizontal axis yields the T_s. As an example, Figure 1c shows the Fredrickson−Larson plots for 15/85 PαMSAN/PMMA blends with and without TRG. An overview of the T_{rheo} and T_s (from eq 4) temperatures is given in Table 1. A comparison is also made in Table 1 with the phase separation temperatures as determined by light microscopy and annealing experiments by Laun[6] for the neat blends.

For the different blends investigated here, the T_{rheo} (obtained from the slope change in G' vs temperature) and the T_s (obtained

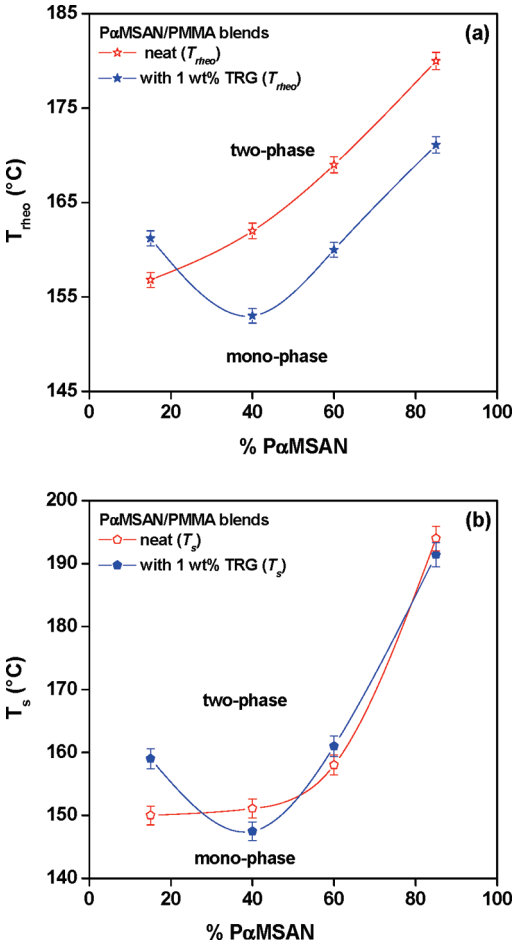

Figure 2. Rheologically determined phase diagram for the neat PαMSAN/PMMA blends and blends with TRG using (a) T_{rheo} (e.g., Figure 1b); (b) T_s (using eq 4).

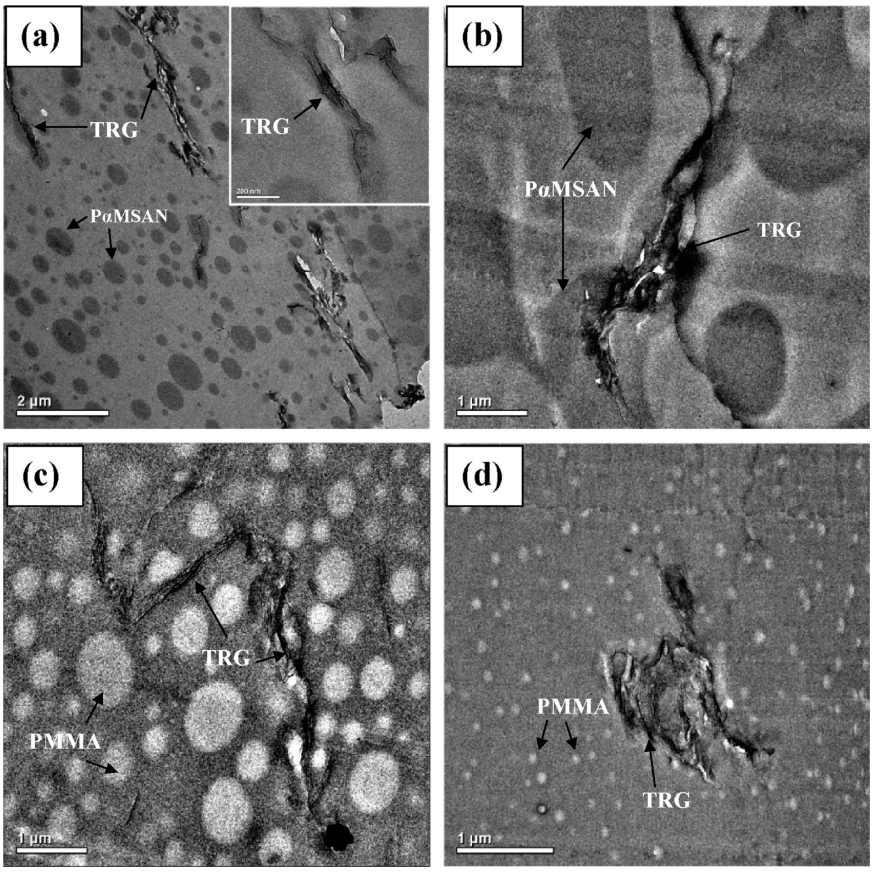

Figure 3. TEM-images of (a) 15/85, (b) 40/60, (c) 60/40, and (d) 85/15 PαMSAN/PMMA blends with TRG. The dark regions are PαMSAN rich domains and the lighter regions are PMMA rich domains.

from eq 4) are plotted as a function of % PαMSAN (wt %) to construct a phase diagram (Figure 2). The lines are only intended as a guide for the eye. The neat blends will be used as a reference to compare the effect of TRG on the phase separation temperature and on the shape of the phase diagram. The concentration of TRG chosen here is well below the percolation threshold which was determined a priori (by small amplitude oscillatory measurements, discussed later in the text). Interestingly, the 40/60, 60/40, and 85/15 PαMSAN/PMMA blends with TRG show an increasing trend in T_{rheo} with PαMSAN concentration which is parallel to the trend of the respective neat blends but approximately 9 °C (±1 °C) lower (see Figure 2a), whereas for the 15/85 PαMSAN/PMMA blend TRG exhibits a delay in phase separation. For the neat blends, the trend for T_s (from eq 4) is quite similar to that of T_{rheo}; however, the absolute values obtained were different (see Figure 2b). It is noteworthy to mention that T_s obtained from Fredrickson Larson plots provides only a rough estimate of the phase separation temperature. To apply the theory, one has to carry out experiments as a function of temperature at very low frequencies (in the terminal zone) of one-phase mixtures in the vicinity of phase transition, which clearly is beyond the practical time scales. The noted differences in T_s and T_{rheo} can hence be attributed to the fact that one can only roughly estimate the T_s from the Fredrickson Larson plots.

Figure 2a suggests that TRG is acting as a nucleating agent thereby inducing phase separation in the composition range beyond 40 wt % PαMSAN in the blends. Nanoclay was also observed to induce phase separation in PMMA/SAN blends.[35] On the contrary, Shumsky et al.[36] reported a delay in phase separation in presence of nanoclay in the same system (PMMA/SAN). Hence, the surface chemistry, the characteristics, the concentration and the positioning of the nanoparticles play a significant role in influencing the thermodynamics of phase separation. In our case, only the 15/85 PαMSAN/PMMA blend with TRG shows a T_{rheo} higher than that of the neat blend. This is also supported by the values obtained from T_s (from eq 4). Thus blends with TRG exhibit a more symmetric phase diagram in contrast to the neat blends (see Figure 2).

Figure 3a–d shows TEM images of the blends with TRG. The darker areas in the images are PαMSAN-rich domains, whereas the lighter areas represent PMMA-rich domains. TRG were observed to be selectively localized in the PαMSAN phase irrespective of the blends composition. It is worth noting that the localization of TRG in a given phase in the blends is driven by thermodynamic forces. The surface free energy (SFE) of PαMSAN can be approximated to either the SFE of α-methyl styrene (γ = 27.4 mN/m at 220 °C) or styrene acrylonitrile with 35% acrylonitrile content (SAN, γ = 34.5 mN/m at 220 °C, % polarity >24).[37] The SFE of PMMA is estimated to be 25.9 mN/m at 220 °C (with % polarity, 28). The SFE of graphene is reported to be 46.7 mN/m.[38] Hence, the localization of TRG can be expected to be energetically favored toward the PαMSAN phase of the blends (i.e., the component having higher SFE). A possible "$\pi-\pi$" interaction between TRG and PαMSAN could

enhance the energetically favored localization of TRG in the PαMSAN phase.[39−41]

Two interesting remarks can be made with respect to the TEM-images. In PMMA-rich blends (15/85 and 40/60), the TRG tend to connect the PαMSAN-rich domains (more clearly visible on the inset of Figure 3a), whereas in PαMSAN-rich blends (60/40 and 85/15), the TRG were observed to be selectively localized in the PαMSAN phase. It is worth noting that similar observations were made in blends with MWNTs, wherein the MWNTs were observed to connect the PαMSAN-rich domains with PαMSAN as the minor phase.[42]

It is envisaged that the adsorbed macromolecular chains result in reduced mobility near the NP surface and on average each polymer chain acquires a stretching energy of $3R_p^2/2Nr_o^2$ (where R_p is the radius of the NP; N, degree of polymerization; r_o, radius of the monomer).[21] The introduction of the nanoparticles hence results in a free energy reduction and stabilization of the homogeneous state,[21] which depends on the concentration of the NPs as well. It is noteworthy that the characteristic dimension of TRG is in the range of 100 nm to 2.5 μm, which is significantly higher than the radius of gyration of the polymer (which is typically of the order of 15−20 nm). Hence, according to the Ginzburg model, a downward shift in the spinodal temperature is expected as the particle rich phase segregates from the polymer even at very low concentrations.[21] We observed that the T_{rheo} of the blends (85/15, 40/60 and 60/40 PαMSAN/PMMA) with TRG is lower by approximately 9 °C (±1 °C) with respect to the neat blends, which can be well-correlated with the Ginzburg model. However, in the 15/85 PαMSAN/PMMA blends, the local filler concentration is expected to be higher as compared to other compositions (at any given loading of TRG) because of selective localization. As a consequence, the effects are quite different as compared to other blends investigated here. It is believed that when the distance between the nanoparticles is comparable to $2R_g$ (radius or gyration of the polymer chains) the mobility of the macromolecular chains is significantly reduced which further prevents phase separation. This often results in higher phase separation temperature and decreased rate of phase separation.[43] Thus, the thermodynamics of the phase separation in PαMSAN/PMMA blends strongly depends on both the composition of the blends and also on the local concentration of TRG in the blends. Temporal evolution of G' would further provide insights in the kinetics of phase separation and is discussed in the next section.

3.2. Kinetics of Phase Separation: Effect of TRG. At isothermal conditions the kinetics of phase separation can be probed by monitoring the evolution of G' as a function of time. In the blends investigated here the kinetics of phase separation were studied at a quench depth well in the spinodal region (220 °C) for both neat as well as for blends with TRG. Figure 4 shows the temporal change in G′ of the neat blends and the blends with 1 wt % TRG, respectively. Changes in G' can be attributed to three major factors: polymer chain dynamics and entanglements from the bulk, concentration fluctuations within the sample and the specific interfacial area of phase separated domains and in addition, the network build up of the TRG in the case of composites. As long as the blend is in the homogeneous regime, the bulk elasticity will dominate the overall value for G'. At a fixed temperature, as time progresses the contribution due to concentration fluctuation increases and at longer time, scales phase separated domains will add elasticity because of increasing interfacial area and will be the dominant factor in the change of G'.[17,44]

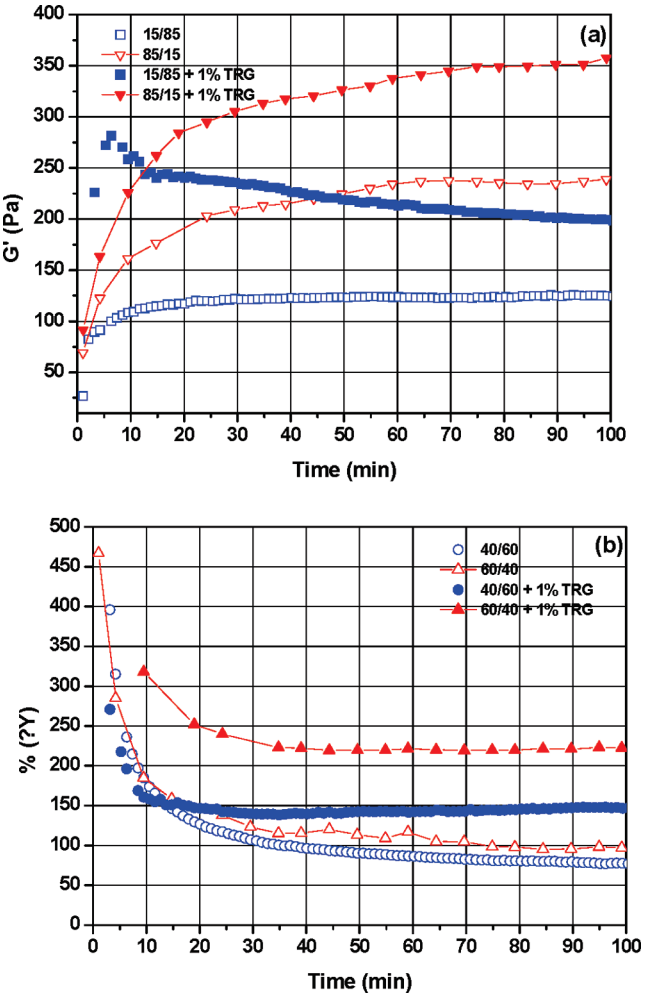

Figure 4. Dynamic time sweeps (after a temperature jump from room temperature to 220 °C with strain 1% and frequency 0.1 rad/s) for PαMSAN/PMMA blends with and without TRG, (a) 15/85 and 85/15 blends; (b) 40/60 and 60/40 blends.

The neat 15/85 and 85/15 PαMSAN/PMMA blends show a similar trend: G' rises as a function of time before a plateau is reached (Figure 4a). When the sample is placed in the rheometer at 220 °C, the initial values for G' are mainly from the concentration fluctuations (early stages of phase separation). Because the 15/85 and 85/15 PαMSAN/PMMA blends phase separate into a droplet-matrix structure,[6] an increase in G' is expected due to the formation of droplet interfaces. As the time passes, the G' stops increasing which indicates that the volume fraction of the droplet phase and the droplet size stays constant and that the concentration fluctuations reaches a steady state. One could expect a decrease in G' due to droplet coalescence by processes like Ostwald ripening. Because of the high viscosity of the polymer matrix and the fact that the volume fraction of the dispersed phase is low, the rate of coarsening is expected to be very slow. For this particular blend, it was reported earlier that the coarsening in dilute blends occurred by Ostwald ripening processes.[28]

On the other hand, the neat 40/60 and 60/40 PαMSAN/PMMA blends show a higher G' initially, followed by a subsequent decrease until a plateau is reached (Figure 4b). It is evident from Figure 4b that for both the blends, we could only pick-up

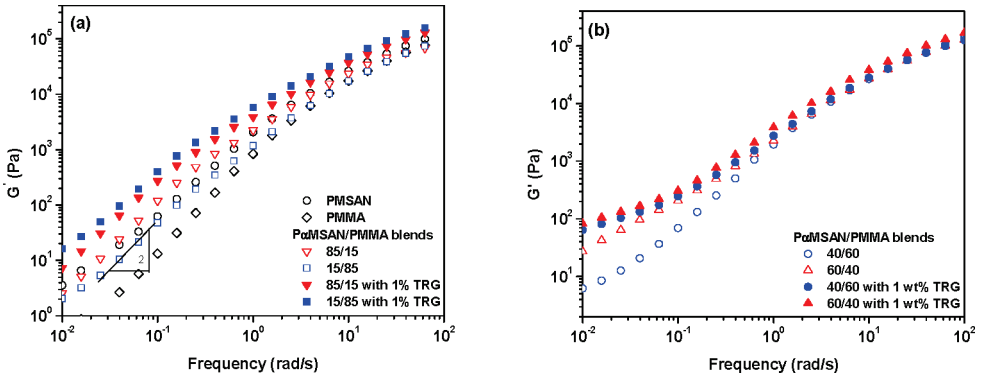

Figure 5. Dynamic frequency sweeps at 220 °C for (a) 15/85 and 85/15 PαMSAN/PMMA blends with TRG and (b) 40/60 and 60/40 PαMSAN/PMMA blends with TRG.

the signals from the late stages of spinodal decomposition i.e. the interfacial tension driven coarsening of cocontinuous structures. The initial rise in G' is caused by the increase in concentration fluctuations. As the phase separation proceeds G' decays as a function of time. This decrease in G′ can be explained by the fact that when a domain gets larger, the volumetric component dominates the viscoelastic properties rather than the interfacial component. During the formation of a cocontinuous structure through spinodal decomposition the structure can be considered to be a network. G' rises during the early stages of phase separation since the elasticity is enhanced by the number of cross-links per unit volume. There is no decrease in G' as long as this network is conserved. When the phase domains coarsen due to interfacial tension, this network is broken up. The loss of interconnectivity leads to a decrease in G'. Further, the storage modulus reaches a plateau when the domains stop growing and the concentration fluctuations saturate. All the blends with TRG reveal higher G' values as compared to the neat blends although the trend of G' as a function of time is roughly the same.

Some important observations can be made. When the 15/85 PαMSAN/PMMA blend with TRG is considered, G' shows an initial rise followed by a subsequent decrease (Figure 4a). This shows that a droplet-matrix structure is formed in the early stages of phase separation, but the droplets undergo coalescence as time progresses. TRG is expected to be selectively localized inside the PαMSAN droplets as the concentration is well below the percolation threshold (see subsequent sections for more detailed analysis). The T_{rheo} for this particular blend is higher than that of the neat blends which essentially indicates that TRG retards the phase separation process. Often a coarse morphology/elongated droplet morphologies are observed when the NPs are selectively localized inside the droplet phases.[42] This is also observed in our case (inset of Figure 3a). As the deformability of the droplets is modified, there is less likelihood of break-up and the domain size increases.[45] It has been reported that NPs can suppress or slow down the rate of coalescence above a certain fraction in the blends.[3,42] Hence, it seems that though the TRG retards the phase separation process at this concentration, the coalescence of the domain is not completely suppressed. A closer look at the time scales reveals that the saturation in G' occurs at a later stage in the blends with TRG as compared to the neat blends. As droplet nucleation and growth are relatively slow processes, it seems that TRG further delays the rate of domain growth, although the coalescence is not arrested at this concentration.

Interestingly, both 40/60 and 60/40 blends show a higher initial value of G' and a decrease as time progresses. It is evident from Figure 4b that for both blends, we could pick up the signals only from the late stages of spinodal decomposition, i.e., the interfacial tension driven coarsening of cocontinuous structures. Similar observations were also reported by Vinckier and Laun.[28] However, for the blends with TRG, the decrease in G' is arrested and a plateau is reached much earlier than that of the neat blends (Figure 4b). This observation essentially indicates that TRG is able to suppress coarsening of the domains in the late stages by acting as a physical barrier. When the kinetics of phase separating blends are observed, a comparison can be made, based on the time scales needed to reach the steady state. The blends with TRG take more time to fully phase separate than the neat blends especially in case of blends with lower fractions of dispersed phases (e.g., 15/85 PαMSAN/PMMA blends). The particles are able to slow down the phase separation kinetics, which is presumably through polymer−particle interaction. The adsorbed macromolecular chains act as a barrier obstructing the motion of the other chains thereby retarding the phase separation process.

In summary, the thermodynamics of the blends in presence of TRG are greatly affected. TRG was observed to induce phase separation in the compositions beyond 40 wt % PαMSAN. On the other hand, TRG was observed to retard phase separation in the case of blends with lower fractions of dispersed phases. This observation was also supported by the time sweep experiments. For instance, at isothermal conditions, a delay in phase separation was observed especially in the case of blends with low fractions of dispersed phases (i.e 15/85 PαMSAN/PMMA blends). Thus, melt-rheology serves as an important tool to understand the thermodynamics and kinetics of phase separation especially in complex materials like TRG filled blends. Temporal evolution of G' at different temperatures (both under metastable and unstable conditions) would provide additional insight on the effects of TRG on kinetics of phase separation and is the subject of future investigations.

3.3. Frequency Sweeps: Percolation Threshold. Dynamic frequency sweeps (in the linear viscoelastic region, determined a priori) were performed (after 5 h) to gain in-depth understanding of the dynamic percolation at elevated temperatures. Panels a and b in Figure 5 illustrates the frequency sweeps for the neat blends and blends with TRG. The 15/85 and 85/15 PαMSAN/PMMA blends show a typical flow region in the low frequency where the G' scales as ω^2, whereas the 40/60 and

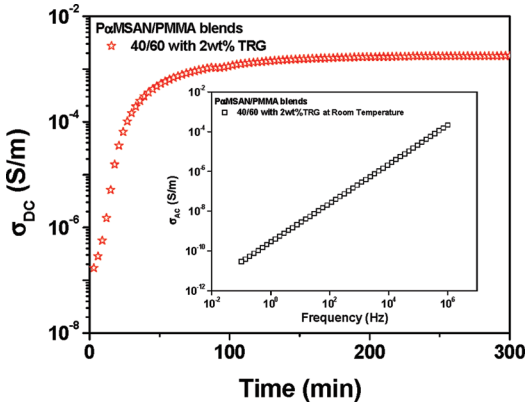

Figure 6. Evolution of DC electrical conductivity as a function of time at 220 °C as the blends phase separate (Inset shows the room temperature conductivity, σ_{AC} versus frequency, of the monophasic composite materials).

60/40 PαMSAN/PMMA blends do not show terminal behavior in the measured frequency window; a typical characteristic of cocontinuous structures.[34] The percolation concentration of filler is often quantified by a plateau in the dynamic moduli at low frequencies. It is evident that for all the blends investigated here the concentration of TRG (1 wt %) seems to be below the rigidity percolation threshold (at least in the measured frequency window), except for a moderate change in the low frequency region of both 40/60 and 60/40 PαMSAN/PMMA blends. From the electron microscopic analysis it was observed that the TRG were not fully exfoliated as one can find few stacked sheets from the TEM images of the final composites. This also suggests relatively poor dispersion of TRG in the THF solution and presumably could be one of the reasons behind the observation of the relatively high percolation threshold. It is worth pointing out that though the concentrations are below the percolation limit in the blends, both the thermodynamics and the kinetics of phase separation were significantly influenced in presence of TRG.

3.4. Electrical Conductivity: Monophasic versus Biphasic Materials. In an earlier study,[42] we reported that phase separation can lead to three-dimensional, MWNT-rich domains in the blends, a feature that provides an alternative strategy for more effective percolation. To investigate this, electrical conductivity spectroscopy measurements (Figure 6) were performed on the 40/60 PαMSAN/PMMA blends in presence of TRG; before phase separation (i.e at room temperature, see inset of Figure 6) and during phase separation at an elevated temperature (220 °C). The experimental details of the conductivity spectroscopy at 220 °C are discussed in the Experimental Section. Interestingly, the monophasic composite sample was an insulator at room temperature, despite the high fraction of TRG (2 wt %), essentially suggesting poor dispersion of the nanoparticles. This was also supported by the TEM analysis where few stacks of sheets were observed in the final composites. Conductivity spectroscopy revealed that the addition of merely 2 wt % TRG is able to transform 40/60 PαMSAN/PMMA blends from virtually insulating at room temperature (monophasic) to a highly conducting material in the melt (biphasic) as a result of phase separation (see Figure 6). Similar observations were also noted for PαMSAN/PMMA blends with MWNTs.[42] At an elevated temperature, the blends phase separate, which allows the nanoparticles to migrate to their specific phase. Such migration during the phase separation leads to an increase in their local concentrations which further assists in their formation of a percolative network-like structure in a given phase. Assuming that all the TRG are localized in a given phase (here PαMSAN), the local concentration of TRG in the 40/60 PαMSAN/PMMA blends is expected to be increased by a factor of ~1.5. This will further facilitate the formation of a networklike structure of TRG. By quenching such microstructures highly conducting materials can be developed at room temperature which otherwise would be insulators. Hence, phase separation can be used as a tool to develop highly conducting materials, which can be further exploited for a wide range of potential applications.

CONCLUSIONS

Thermally induced phase separation in an LCST-type blend has been monitored in the presence of TRG by melt-rheology and electrical conductivity spectroscopy. The concentration of TRG studied here is well below the rigidity percolation threshold which was determined a priori. The evolution of the dynamic modulus as a function of temperature and time was used as a tool to gain in-depth understanding of the phase separation process in presence of TRG. The thermodynamics of phase separation was significantly influenced in presence of TRG. Except for 15/85 PαMSAN/PMMA blends, TRG was observed to act as a nucleating agent inducing phase separation. Furthermore, TRG was observed to influence the rate of phase separation as evidenced from the temporal evolution of the dynamic modulus. The state of dispersion of TRG in the blends was assessed by electron microscopy and conductivity spectroscopy measurements. The monophasic composite samples with 2 wt % TRG were virtually insulators at room temperature, whereas biphasic materials were observed to be highly conducting in the melt. This phenomenon offers routes to tailor the material properties for a wide range of potential applications.

AUTHOR INFORMATION

Corresponding Author

*Fax: +32 16 322991. E-mail: paula.moldenaers@cit.kuleuven.be.

Present Address

[||]Department of Materials Engineering, Indian Institute of Science, Bangalore-560012, India.

ACKNOWLEDGMENT

Onderzoeksfonds K.U. Leuven (Postdoctoral Fellowship for S.B. and GOA 09/2002) and Research Foundation-Flanders, FWO (Postdoctoral Fellowship for J.L.), are gratefully acknowledged for the financial support. We thank Yu-qiang Qian (University of Minnesota) for collecting the TEM images.

REFERENCES

(1) Fenouillot, F.; Cassagnau, P.; Majeste, J. C. *Polymer* **2009**, *50* (6), 1333–1350.

(2) Bose, S.; Khare, R. A.; Moldenaers, P. *Polymer* **2010**, *51* (5), 975–993.

(3) Vermant, J.; Cioccolo, G.; Nair, K. G.; Moldenaers, P. *Rheol. Acta* **2004**, *43* (5), 529–538.

(4) Vandebril, S.; Vermant, J.; Moldenaers, P. *Soft Matter* **2010**, *6*, 3353–3362.

(5) Gunton, J. D.; San Miguel, M.; Sahni, P. In *Phase Transitions and Critical Phenomenon*; Lebowitz, J. L., Ed.; Academic Press: London, 1983; Vol. 8.
(6) Laun, H. M. *Pure Appl. Chem.* **1998**, *70* (8), 1547–1566.
(7) Ougizawa, T.; Inoue, T. *Polym. J.* **1986**, *18* (7), 521–527.
(8) Ajji, A.; Choplin, L. *J. Polym. Sci., Part B: Polym. Phys.* **1988**, *26* (11), 2279–2289.
(9) Chopra, D.; Vlassopoulos, D.; Hatzikiriakos, S. G. *J. Rheol.* **2000**, *44* (1), 27–45.
(10) Kapnistos, M.; Hinrichs, A.; Vlassopoulos, D.; Anastasiadis, S. H.; Stammer, A.; Wolf, B. A. *Macromolecules* **1996**, *29* (22), 7155–7163.
(11) Madbouly, S. A.; Ougizawa, T.; Inoue, T. *Macromolecules* **1999**, *32* (17), 5631–5636.
(12) Mani, S.; Malone, M. F.; Winter, H. H. *J. Rheol.* **1992**, *36* (8), 1625–1649.
(13) Vlassopoulos, D.; Koumoutsakos, A.; Anastasiadis, S. H.; Hatzikiriakos, S. G.; Englezos, P. *J. Rheol.* **1997**, *41* (3), 739–755.
(14) Li, Z. H.; Zhang, X. M.; Tasaka, S.; Inagaki, N. *Mater. Lett.* **2001**, *48* (2), 81–88.
(15) Li, J. G.; Li, H. Y.; Wu, C. H.; Ke, Y. C.; Wang, D. J.; Li, Q.; Zhang, L. Y.; Hu, Y. L. *Eur. Polym. J.* **2009**, *45* (9), 2619–2628.
(16) Wang, K. Y.; Chen, Y. M.; Zhang, Y. *Polymer* **2008**, *49* (15), 3301–3309.
(17) Sharma, J.; Clarke, N. *J. Phys. Chem. B* **2004**, *108* (35), 13220–13230.
(18) Austin, J. R.; Kontopoulou, M. *Polym. Eng. Sci.* **2006**, *46* (11), 1491–1501.
(19) Fredrickson, G. H.; Larson, R. G. *J. Chem. Phys.* **1987**, *86* (3), 1553–1560.
(20) Baudouin, A. C.; Devaux, J.; Bailly, C. *Polymer* **2010**, *51* (6), 1341–1354.
(21) Ginzburg, V. V. *Macromolecules* **2005**, *38* (6), 2362–2367.
(22) Jeon, H. K.; Macosko, C. W. *Polymer* **2003**, *44* (18), 5381–5386.
(23) Gharachorlou, A.; Goharpey, F. *Macromolecules* **2008**, *41* (9), 3276–3283.
(24) Hore, M. J. A.; Laradjii, M. *MRS Symp. Proc.* **2005**, *856E*, BB7.7.
(25) Schniepp, H. C.; Li, J. L.; McAllister, M. J.; Sai, H.; Herrera-Alonso, M.; Adamson, D. H.; Prud'homme, R. K.; Car, R.; Saville, D. A.; Aksay, I. A. *J. Phys. Chem. B* **2006**, *110* (17), 8535–8539.
(26) Ramanathan, T.; Abdala, A. A.; Stankovich, S.; Dikin, D. A.; Herrera-Alonso, M.; Piner, R. D.; Adamson, D. H.; Schniepp, H. C.; Chen, X.; Ruoff, R. S.; Nguyen, S. T.; Aksay, I. A.; Prud'homme, R. K.; Brinson, L. C. *Nature Nanotechnol.* **2008**, *3* (6), 327–331.
(27) Kim, H.; Abdala, A. A.; Macosko, C. W. *Macromolecules* **2010**, *43* (16), 6515–6530.
(28) Vinckier, I.; Laun, H. M. *Rheol. Acta* **1999**, *38* (4), 274–286.
(29) McAllister, M. J.; Li, J. L.; Adamson, D. H.; Schniepp, H. C.; Abdala, A. A.; Liu, J.; Herrera-Alonso, M.; Milius, D. L.; Car, R.; Prud'homme, R. K.; Aksay, I. A. *Chem. Mater.* **2007**, *19* (18), 4396–4404.
(30) Alig, I.; Lellinger, D.; Dudkin, S. M.; Potschke, P. *Polymer* **2007**, *48* (4), 1020–1029.
(31) Serwadczak, M.; Wubbenhorst, M.; Kucharski, S. *J. Non-Cryst. Solids* **2007**, *353* (47−51), 4303–4312.
(32) Wubbenhorst, M.; van Turnhout, J. *J. Non-Cryst. Solids* **2002**, *305* (1−3), 40–49.
(33) Huang, Y. J.; Jiang, S. J.; Li, G. X.; Chen, D. H. *Acta Mater.* **2005**, *53* (19), 5117–5124.
(34) Ajji, A.; Choplin, L.; Prudhomme, R. E. *J. Polym. Sci., Part B: Polym. Phys.* **1991**, *29* (13), 1573–1578.
(35) Lee, M.; Lee, K.; Min, B. H.; Kim, J. H. *J. Appl. Polym. Sci.* **2010**, *117* (1), 49–57.
(36) Shumsky, V. F.; Getmanchuk, I.; Ignatova, T.; Maslak, Y.; Cassagnau, P.; Boiteux, G.; Melis, F. *Rheol. Acta* **2010**, *49* (8), 827–836.
(37) Solid surface energy data (SFE) for common polymers. http://www.surface-tension.de/solid-surface-energy.htm.
(38) Wang, S. R.; Zhang, Y.; Abidi, N.; Cabrales, L. *Langmuir* **2009**, *25* (18), 11078–11081.
(39) Malig, J.; Jux, N.; Kiessling, D.; Cid, J.-J.; Vázquez, P.; Torres, T.; Guldi, D. M. *Angew. Chem., Int. Ed.* **2011**, *50* (15), 3561–3565.
(40) Zhang, H.; Lee, H. K. *J. Chromatogr., A* **2011**, *1218* (28), 4509–4516.
(41) Yang, Z.; Shi, X.; Yuan, J.; Pu, H.; Liu, Y. *Appl. Surf. Sci.* **2010**, *257* (1), 138–142.
(42) Bose, S.; Özdilek, C.; Leys, J.; Seo, J. W.; Wübbenhorst, M.; Vermant, J.; Moldenaers, P. *ACS Appl. Mater. Interfaces* **2010**, *2* (3), 800–807.
(43) Lipatov, Y. S.; Nesterov, A. E.; Ignatova, T. D.; Nesterov, D. A. *Polymer* **2002**, *43* (3), 875–880.
(44) Zhang, Z. L.; Zhang, H. D.; Yang, Y. L.; Vinckier, I.; Laun, H. M. *Macromolecules* **2001**, *34* (5), 1416–1429.
(45) Dasari, A.; Yu, Z. Z.; Mai, Y. W. *Polymer* **2005**, *46* (16), 5986–5991.